ELSEVIER

Journal of Nuclear Materials 254 (1998) 34–41

journal of nuclear materials

Thermal stability and brazing characteristics of Zr–Be binary amorphous filler metals for zirconium alloy

Choon-Ho Park [a], Young-Soo Han [a], Yoon-Kee Kim [b], Kuk-Jin Jang [a], Jai-Young Lee [a,*], Chang-Burm Choi [c], Ki-Seob Sim [d]

[a] *Department of Materials Science and Engineering, Korea Advanced Institute of Science and Technology, Kusong-Dong 373-1, Yusung-Gu, Taejon 305-701, South Korea*

[b] *Plasma Technology Center, R&D Planning Division, Institute for Advanced Engineering, Yongin, P.O. Box 25, Kyonggi-do, South Korea*

[c] *Fuel Technology Center, Korea Nuclear Fuel Co., Ltd, 150 Duckjin-Dong, Yusung-Gu, Taejon, South Korea*

[d] *CANFLEX Fuel Development, Korea Atomic Energy Research Institute, 150 Duckjin-Dong, Yusung-Gu, Taejon, South Korea*

Received 30 July 1997; accepted 9 November 1997

Abstract

The thermal stability and brazing characteristics of Zr–Be binary amorphous alloys as a new filler metal for joining zirconium alloy were investigated in order to supersede physically vapor-deposited (PVD) beryllium used conventionally with many disadvantages. The $Zr_{1-x}Be_x$ $(0.3 \leq x \leq 0.5)$ binary amorphous alloys were produced by melt-spinning method. In the selected composition range the Zr–Be amorphous alloys have two crystallization modes which are dependent on beryllium content in alloys. The temperatures and activation energies for crystallization depend on crystallization-mode as well as beryllium content. These amorphous alloys were put into practical use in joining bearing pads on zircaloy cladding sheath. Using Zr–Be amorphous alloys as filler metals, the reduction in thickness of cladding sheath wall are prevented. Especially, in the case of using $Zr_{0.65}Be_{0.35}$ and $Zr_{0.7}Be_{0.3}$ amorphous alloys, smooth interface and spherical primary α-Zr particles appear in the brazed layer, which is desirable microstructure in the view of the corrosion–resistance. © 1998 Elsevier Science B.V.

1. Introduction

In the manufacture of CANDU and CANFLEX fuel bundles, various components (spacer pads, bearing pads, buttons) are joined by a brazing process on the surface of the cladding sheath made with zirconium alloy [1]. Physically vapor-deposited (PVD) metallic beryllium has been used currently as a brazing filler metal [2]. In this case, the chemical toxicity of beryllium vapor requires a very complicated PVD process for physical protection [3]. Moreover, there are several shortcomings such as the reduction of the sheath wall and difficulty of microstructural control due to the nature of diffusion brazing [4,5]. At first, zirconium–beryllium (Zr–Be) binary crystalline alloys were used as brazing filler metals. However its brittleness and difficulty in handling during the joining process resulted in unsound brazing [6]. Therefore, Zr–Be amorphous alloys have been selected as other filler metals for joining zircaloy. In particular Zr–Be alloy has an eutectic composition (Be = 35a/o), so that it has a low melting temperature and good amorphous formability [7–10].

There have been numerous researches on the applications of metallic amorphous alloys for brazing filler metals [11,12]. The rapidly solidified amorphous alloys offer superior chemical and microstructural homogeneity. The ductility of metallic glass alloys enables themselves to deform for direct application. In brazing, the amorphous filler metals can be inserted as an interlayer between the base metals. This does not only eliminate the dependence on capillary action to convey filler metal throughout the joint area but also prevents the erosion of base metals [13].

In this work, the amorphous formability and the thermal stability of Zr–Be amorphous alloys are investigated.

* Corresponding author. Tel.: +82-42 869 3313; fax: +82-42 869 8910; e-mail: jailee@sorak.kaist.ac.kr.

PII S0022-3115(97)00345-0

The joints brazed by using PVD Be metal and Zr–Be amorphous alloys are compared in view of microstructural standpoints. It is hoped that the Zr–Be amorphous filler metal is able to overcome a lot of disadvantages caused by the use of conventional PVD beryllium metal. The Zr–Be binary amorphous alloys applicable to the joining zirconium alloys are suggested.

2. Experimental

The $Zr_{1-x}Be_x$ alloys, where x ranged from 0.3 to 0.5, were prepared from materials with 99.9 w/o purity by means of arc-melting under an inert atmosphere of argon. These alloys were remelted three times for homogeneity. These are from hypo-eutectic to hyper-eutectic compositions of Zr–Be binary alloy system. Amorphous ribbons were prepared by the melt-spinning method [14,15] under a low pressure of argon. The alloys were heated to about 1000°C (above the corresponding liquidus temperature) in a quartz tube by high frequency induction heating and injected by argon pressure of 0.7 atm onto the copper wheel which was turning at a tangential speed of 32 m/s in the Ar atmosphere to prevent the oxidation of ribbons. The thickness and width of the ribbons were about 40 μm and 2 mm, respectively.

The amorphization of these ribbons was examined by an X-ray diffractometer (Rigaku D/MAX-IIIC) with Cu-Kα radiation and by transmission electron microscopy (TEM; Phillips CM20). In order to examine the crystallization behavior and the thermal stability of the amorphous ribbons, thermal analysis was conducted using a differential scanning calorimeter (Perkin–Elmer DSC-4). The amorphous ribbons were heated from 30 to 500°C at heating rates of 10, 20, 30 and 50°C/min.

After the amorphous ribbon was located between a bearing pad ($2.5 \times 30 \times 1.5$ mm) and a Zircaloy-4 cladding sheath which is a tube of 0.4 mm thick and 13 mm diameter, the pad was temporarily and mechanically joined onto the sheath by a press. Brazing was then carried out under 10^{-5} Torr at 1050°C for 20 s. Six types of filler metals which are physically vapor-deposited (PVD) beryllium and $Zr_{1-x}Be_x$ ($x = 0.3$, 0.35, 0.4, 0.45 and 0.5) were used as filler metals. The microstructures of the brazed layer were examined metallographically by optical microscopy and scanning electron microscopy to evaluate the thickness and morphology of the brazed layer with respect to the composition of the filler metals.

3. Results and discussion

3.1. The formation and thermal stability of $Zr_{1-x}Be_x$ ($0.3 \le x \le 0.5$) amorphous alloys

The X-ray diffraction (XRD) patterns of the Zr–Be ribbons made by the melt-spinning method are shown in Fig. 1. There are no distinguishable peaks in these patterns over all experimental compositions except a broad peak centered in the vicinity of 36° observed from all XRD patterns. The TEM diffraction patterns of the ribbons show a diffuse halo-ring, as shown in Fig. 2. From the above

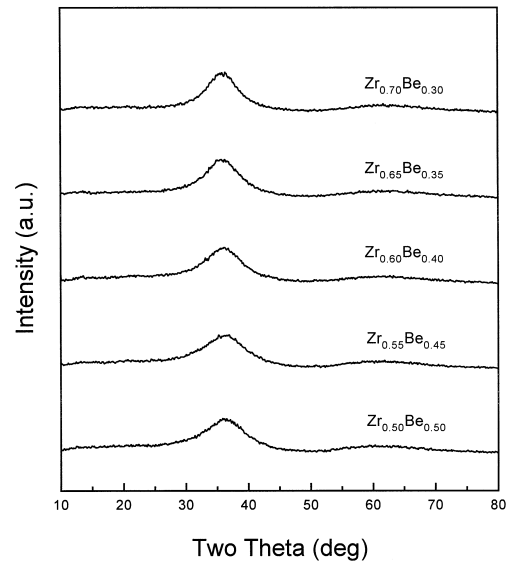

Fig. 1. X-ray diffraction patterns of $Zr_{1-x}Be_x$ ($x = 0.3$, 0.35, 0.4, 0.45, 0.5) ribbons prepared by melt-spinning.

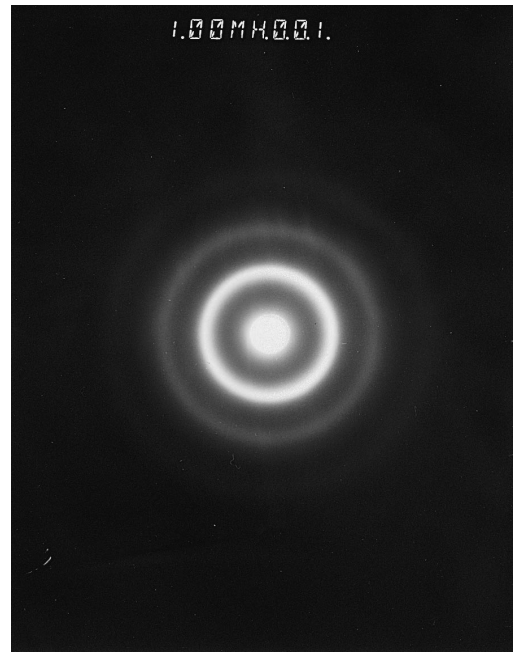

Fig. 2. TEM diffraction pattern of $Zr_{0.7}Be_{0.3}$ ribbon prepared by melt-spinning.

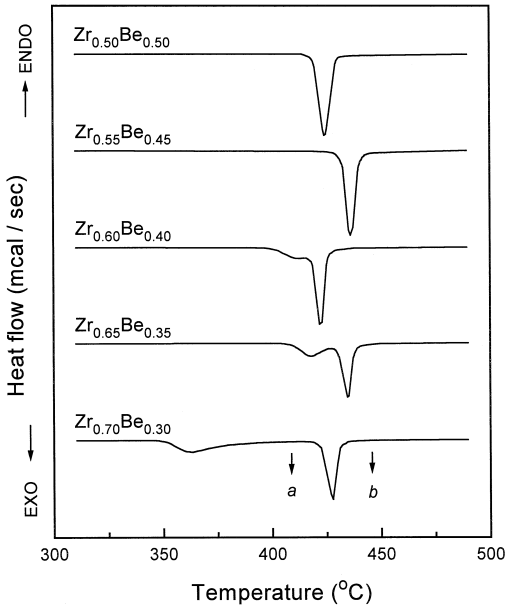

Fig. 3. DSC curves of amorphous $Zr_{1-x}Be_x$ ($x = 0.3$, 0.35, 0.4, 0.45, 0.5) alloys at 20°C/min heating rate.

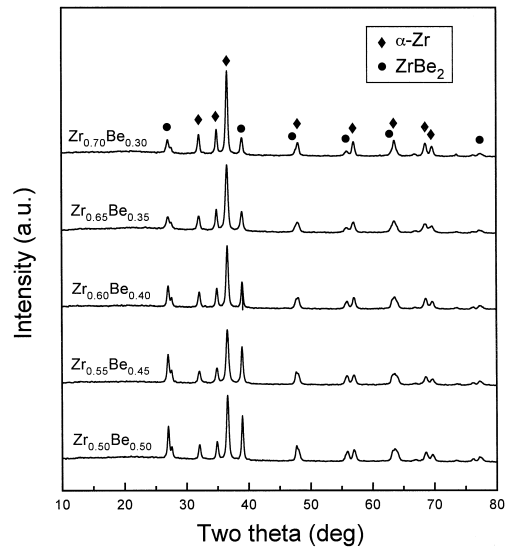

Fig. 4. X-ray diffraction patterns of fully crystallized $Zr_{1-x}Be_x$ ($x = 0.3$, 0.35, 0.4, 0.45, 0.5) alloys.

results, it is confirmed that the ribbons prepared by melt-spinning are amorphous alloys.

The DSC results obtained from the ribbons having a different amount of Be are shown in Fig. 3. In the case of $Zr_{0.5}Be_{0.5}$ and $Zr_{0.55}Be_{0.45}$ amorphous alloys, single exothermic peak is observed. The others have double exothermic peaks. The presence of single peak in the DSC curve means the direct transformation from the amorphous phase to stable crystalline phase. The occurrence of double peaks implies that the formation of stable crystalline phases is conducted by two step processes. In the first step, the amorphous phase is transformed into the metastable phase or stable crystalline phase plus another amorphous phase. In the second step, the intermediate phases transform into final equilibrium phases. In order to analyze the final crystalline phases transformed from $Zr_{1-x}Be_x$ ($0.3 \leq x \leq 0.5$) alloys, XRD patterns of the samples rapidly quenched from the temperature of the peak tails, which means the end of crystallization, in the DSC curve were examined. From comparison with the JCDPS [16], it is found that the final stable crystalline phases transformed from the amorphous alloys are α-Zr and $ZrBe_2$, as shown in Fig. 4, regardless of both the composition of alloys and the number of peaks in DSC curve. The relative XRD intensity ratio of α-Zr to $ZrBe_2$ peaks increases with the content of zirconium in the alloys.

After the amorphous ribbons of $Zr_{0.7}Be_{0.3}$ alloys were heated up to the end of the first peak (point a in Fig. 3) and were immediately quenched to room temperature, they were analyzed by an X-ray diffractometer in order to investigate the two step crystallization process. The XRD of the $Zr_{0.7}Be_{0.3}$ alloys which were heated up to the end of the second peak (point b in Fig. 3) and quenched immediately was also measured. The XRD results obtained from the samples quenched at temperature a and b are shown in Fig. 5. The crystalline phase formed at a relatively low temperature is revealed as α-Zr from comparison with the data in JCPDS. In the XRD pattern obtained from the sample quenched after the relatively high temperature peak

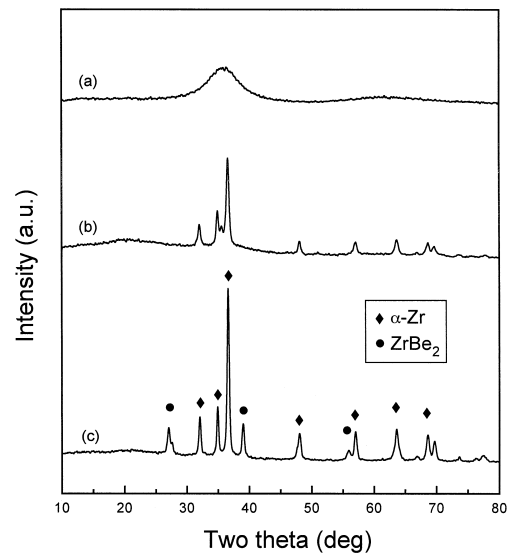

Fig. 5. X-ray diffraction patterns of $Zr_{0.7}Be_{0.3}$ alloys; (a) as-received ribbons from melt-spinning, (b) after first reaction (quenched from a in Fig. 3), (c) after full crystallization (quenched from *b* in Fig. 3).

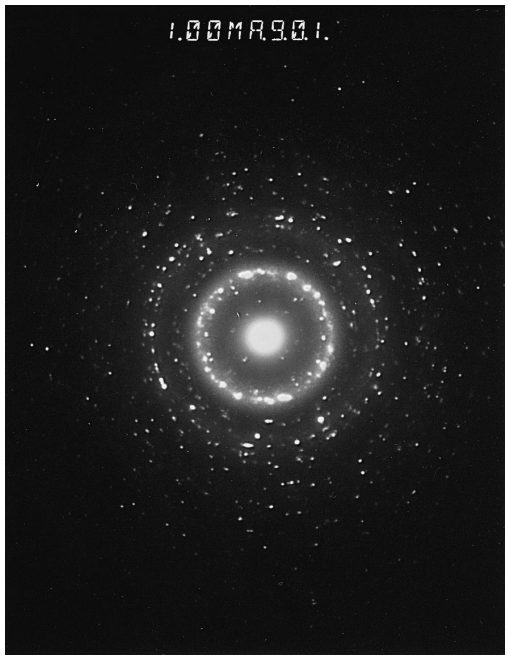

Fig. 6. TEM diffraction pattern of $Zr_{0.7}Be_{0.3}$ alloy after first reaction (quenched from a in Fig. 3).

(at temperature b), there are new peaks which were not observed in the XRD measured from the sample quenched at temperature a. By indexing the peaks using the JCPDS, the new peaks prove to be the $ZrBe_2$ phase. The TEM diffraction pattern measured from the samples quenched at temperature a shows both diffuse halo-ring and broad spots here and there as shown in Fig. 6. Therefore, the crystallization process of the amorphous $Zr_{0.7}Be_{0.3}$ alloys which have two exothermic peaks in the DSC curve consists of the first step in which the amorphous Zr–Be alloy transforms to the α-Zr phase plus another amorphous phase at a relatively low temperature and the second step in which the $ZrBe_2$ phase is formed from them at a relatively high temperature.

The crystallization temperatures (T_x) as a function of beryllium content are shown in Table 1. It is found that the crystallization temperatures of the amorphous $Zr_{1-x}Be_x$ alloys in the composition range of $0.3 \le x \le 0.5$ are independent of the content of beryllium.

Table 1
Crystallization temperature T_x (K) and activation energy ΔE_x (kcal/mol) for the crystallization reactions of Zr–Be amorphous alloys

Composition	T_x (K)		ΔE_x (kcal/mol)	
	T_{x1}	T_{x2}	ΔE_{x1}	ΔE_{x2}
$Zr_{0.70}Be_{0.30}$	624	697	54.35	77.50
$Zr_{0.65}Be_{0.35}$	683	704	55.61	73.88
$Zr_{0.60}Be_{0.40}$	676	692	51.71	65.46
$Zr_{0.55}Be_{0.45}$		706		61.55
$Zr_{0.50}Be_{0.50}$		693		62.84

The activation energy (ΔE_x) of a crystallization reaction can be determined by the Kissinger method [17]:

$$\mathrm{d}\ln\left(\phi/T_\mathrm{p}^2\right)/\mathrm{d}\left(1/T_\mathrm{p}\right) = -\Delta E_x/R,$$

where ϕ is the heating rate, T_p is the peak temperature in the DSC curve and R is the gas constant. The Kissinger plots of the first and second exothermic reactions are shown in Fig. 7. The activation energies calculated from

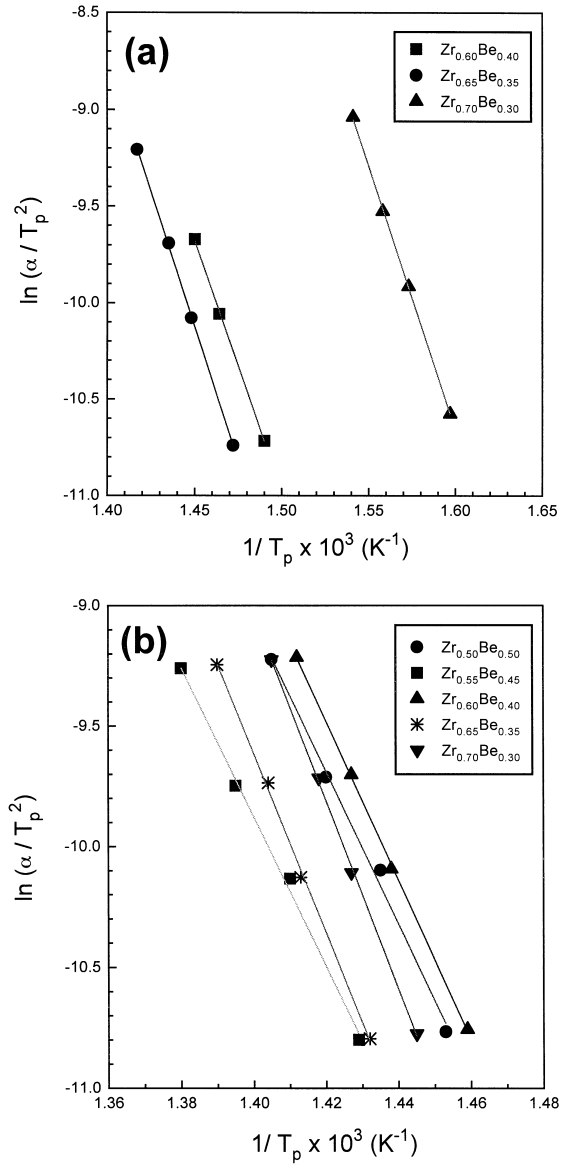

Fig. 7. Kissinger plots (a) for the first peak reaction of $Zr_{1-x}Be_x$ ($x = 0.3$, 0.35, 0.4) alloys (b) for the second peak reaction of $Zr_{1-x}Be_x$ ($x = 0.3$, 0.35, 0.4, 0.45, 0.5) alloys in DSC.

the slope of these plots are presented in Table 1. The activation energy for the formation of α-Zr is about 54 kcal/mol and that of $ZrBe_2$ is about 72 kcal/mol. The activation energy for the crystallization of the $Zr_{0.55}Be_{0.45}$ and $Zr_{0.5}Be_{0.5}$ alloys which have only one crystallization reaction is almost the same as the average value of the activation energy of the first and the second crystallization of the $Zr_{0.7}Be_{0.3}$, $Zr_{0.65}Be_{0.35}$ and $Zr_{0.6}Be_{0.4}$ alloys. From the X-ray analysis as shown in Fig. 4, the crystalline phases from the $Zr_{0.55}Be_{0.45}$ and $Zr_{0.5}Be_{0.5}$ alloys after annealing are the α-Zr and $ZrBe_2$ phases. Therefore, it can be said that the two amorphous alloys simultaneously transform to the α-Zr phase and $ZrBe_2$ phase with an activation energy of about 62 kcal/mol. From the above results, the $Zr_{1-x}Be_x$ $(0.3 \leq x \leq 0.5)$ amorphous alloys are separated into two groups by crystallization behavior. The $Zr_{0.55}Be_{0.45}$ and $Zr_{0.5}Be_{0.5}$ alloys are crystallized by the eutectic crystallization to form simultaneously the α-Zr and $ZrBe_2$ phases. In the case of the other three amorphous alloys the crystalline α-Zr phase emerges in the amorphous matrix at the first peak temperature and then the remaining amorphous alloy transforms to the $ZrBe_2$ phase at the second peak temperature.

3.2. Microstructure of the brazements

Bearing pads were brazed on the surface of the cladding sheath with $Zr_{1-x}Be_x$ $(0.3 \leq x \leq 0.5)$ amorphous ribbons

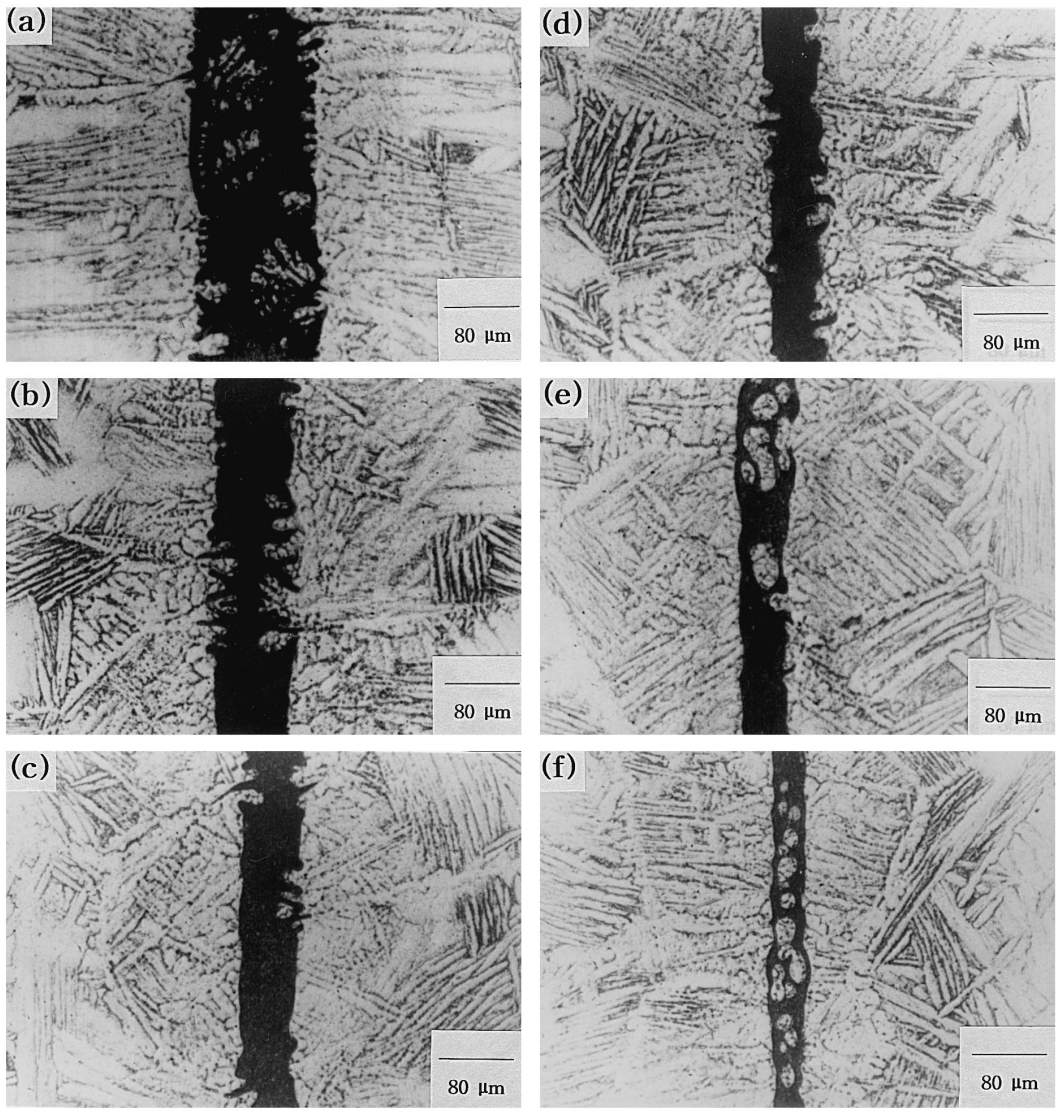

Fig. 8. Optical photographs of the interfaces brazed with (a) Be metal film, (b) $Zr_{0.5}Be_{0.5}$, (c) $Zr_{0.55}Be_{0.45}$, (d) $Zr_{0.6}Be_{0.4}$, (e) $Zr_{0.65}Be_{0.35}$ and (f) $Zr_{0.7}Be_{0.3}$ amorphous ribbons as filler metals.

of 40 μm thickness as filler metals at 1050°C. The microstructures of the brazed layers are shown in Figs. 8 and 9. For comparison, the microstructures of the layer brazed with PVD metallic beryllium, which is a filler metal currently used to join bearing pads on the Zircaloy-4 cladding sheath in the nuclear fuel reactor, are also shown in Figs. 8 and 9.

In the case of using the PVD metallic Be with 20 μm thickness, the width of the brazed layer is about 80 μm, as shown in Fig. 8(a) and Fig. 9(a). The melting temperatures of Be and Zr are 1289 and 1855°C, respectively. However, the eutectic temperature of the Zr and $ZrBe_2$ is 965°C [18,19]. As the composition of the Zircaloy cladding sheath made contact with the PVD, Be reached almost the eutectic point by the diffusion of Be atoms into the sheath and the alloys in the contact zone which was near the eutectic composition began to melt into the liquid phase at 1050°C. This liquid fills up the brazing gap and solidifies by cooling. Solidification of the melt starts at the cladding wall and forms a dendrite structure as shown in Fig. 9(a).

On the other hand, in the case using the Zr–Be amorphous ribbons there was no remarkable increase in the width of the brazed layer to compare with the original thickness of the filler metals. So, the erosion of the cladding wall can be prevented by application of the Zr–Be amorphous filler metals in the brazing process. There is only a small difference in the width of the brazed layer depending on the content of beryllium in the amor-

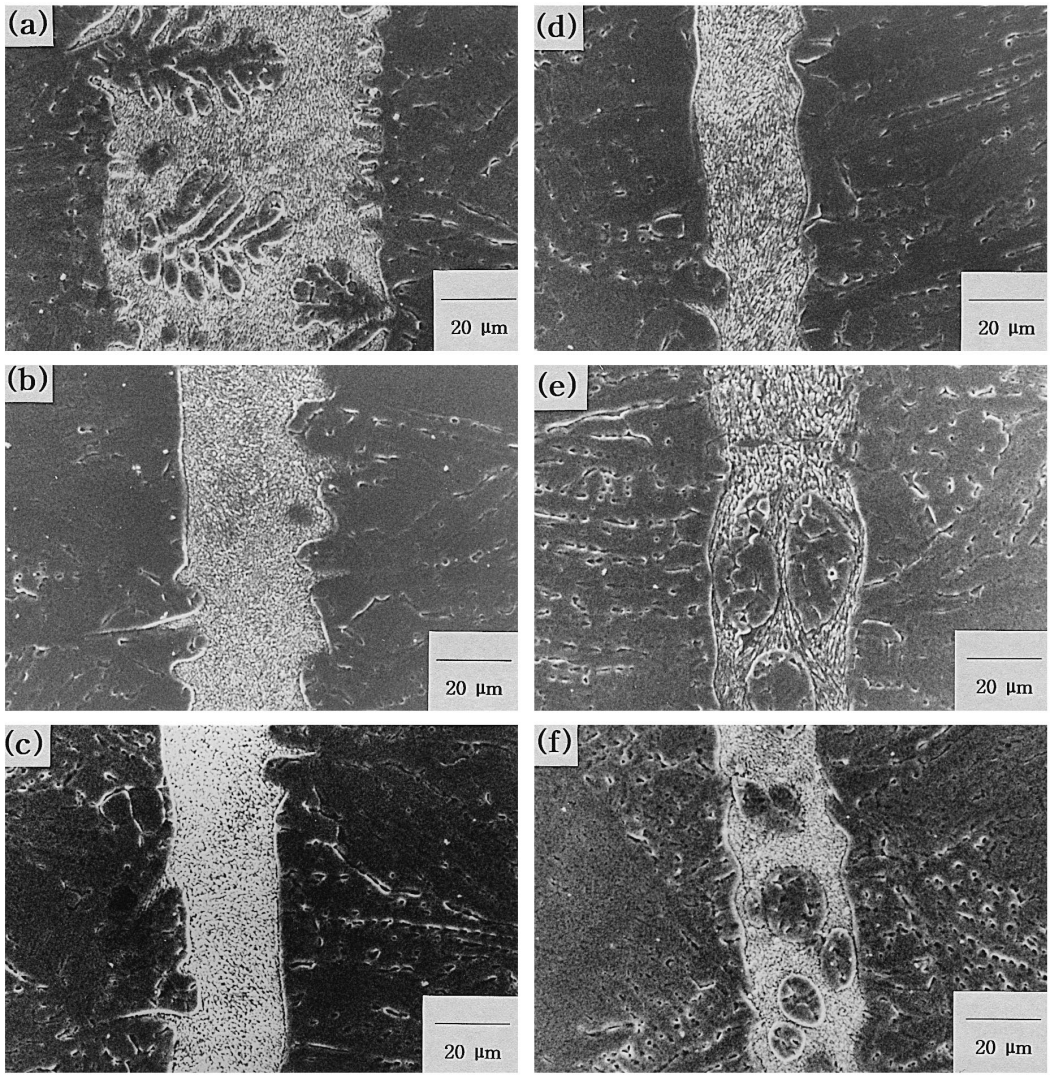

Fig. 9. SEM photographs of the interfaces brazed with (a) Be metal film, (b) $Zr_{0.5}Be_{0.5}$, (c) $Zr_{0.55}Be_{0.45}$, (d) $Zr_{0.6}Be_{0.4}$, (e) $Zr_{0.65}Be_{0.35}$ and (f) $Zr_{0.7}Be_{0.3}$ amorphous ribbons as filler metals.

phous ribbons. Increasing the content of Be in the amorphous alloys, the concentration gradient of Be between the ribbons and the cladding sheath becomes larger and the diffusion of Be atoms to the wall is promoted. Therefore, the thickness of the brazed layer is relatively thick using the Zr–Be amorphous ribbons with a relatively large amount of beryllium as shown in Fig. 8.

Brazed interface layers consist of a eutectic matrix and primary particles. According to the equilibrium phase diagram of the Zr–Be binary system [18,19], island particles in the eutectic bed are primary α-Zr for hypo-eutectic compositions and primary $ZrBe_2$ for hyper-eutectic compositions, respectively. Using the PVD metallic Be as a filler material, there are well developed dendrite structures in the brazed layer as shown in Fig. 9(a).

In the case of hyper-eutectic compositional ribbons which contain a relatively large amount of Be in alloys, the interface between the cladding sheath and the brazed layer is rough and the dendrite structure which grows from the interface into the brazed layer appears as shown in Fig. 8(b), (c) and (d). The diffusion of beryllium atoms toward the zircaloy causes the formation of a liquid alloy at 1050°C. As solidification proceeds the equilibrium primary particles will be produced from the liquid alloy in the brazed gap by nucleation at the interfaces of the cladding sheath/liquid and growth into the brazed gap. So, the dendrite structure in the eutectic bed appears.

Using the hypo-eutectic compositional amorphous alloys as filler materials, the smooth interface and spherical particles are formed in the eutectic bed as shown in Fig. 8(e) and (f) and Fig. 9(e) and (f). The thickness of the brazed layer is smaller using hypo-eutectic compositional materials than using hyper-eutectic ones. Therefore, the decrease in the thickness of the cladding wall by brazing can be reduced by using the amorphous Zr–Be binary alloys with hypo-eutectic composition. In the case of $Zr_{0.7}Be_{0.3}$ and $Zr_{0.65}Be_{0.35}$ amorphous alloys which have a hypo-eutectic composition, the liquid phase is formed by melting down of the amorphous filler metals at 1050°C. With decreasing temperature, the equilibrium phases of the filler metals change from liquid to another liquid and isolated primary particles. Because the primary particles are surrounded by isotropic liquid alloy, the spherical shape of the particles is produced in the eutectic bed to minimize the interface energy between the particles and liquid phase.

From the microstructural evolution of the brazed joints with the change of composition in amorphous $Zr_{1-x}Be_x$ $(0.3 \le x \le 0.5)$ filler materials, it is found that the morphology of brazed layers can be easily controlled without the change of other brazing parameters if Zr–Be amorphous filler metals are used.

In respect to the corrosion behavior of brazed layers, it is known that the corrosion rate of $ZrBe_2$ is faster than that of α-zirconium [20]. This fact proves that the corrosion resistance of brazed joints in the nuclear fuel reactor will be enhanced when the brazed layer has primary α-Zr particles in the eutectic bed.

From the above results, the $Zr_{0.7}Be_{0.3}$ amorphous alloy is the best filler metal for the joining of zirconium alloys from the viewpoint of corrosion resistance.

4. Conclusions

$Zr_{1-x}Be_x$ binary amorphous alloys in the composition range of $0.3 \le x \le 0.5$ were produced by the melt-spinning method. The $Zr_{1-x}Be_x$ amorphous alloys could be separated into two groups by crystallization behavior. The $Zr_{0.55}Be_{0.45}$ and $Zr_{0.5}Be_{0.5}$ alloys were crystallized by eutectic crystallization to form simultaneously α-Zr and $ZrBe_2$ phase. In the case of $Zr_{0.6}Be_{0.4}$, $Zr_{0.65}Be_{0.35}$ and $Zr_{0.7}Be_{0.3}$ amorphous alloys, the crystalline α-Zr phase is formed at the first peak temperature (at a relatively low temperature; about 380°C) and the remaining amorphous phase transformed to the $ZrBe_2$ phase at the second peak temperature (at a relatively high temperature; about 430°C) of DSC curve.

The thickness of the brazed layer using the Zr–Be amorphous alloy was thinner than that using the PVD Be metal. In the case of using hyper-eutectic compositional ribbons which contained relatively large amount of Be in alloys, a rough interface between the cladding sheath and the brazed layer appeared and a dendrite structure grew from the interface into the brazed layer. Using the hypo-eutectic compositional amorphous alloys, $Zr_{0.7}Be_{0.3}$ and $Zr_{0.65}Be_{0.35}$, the smooth interface and spherical shape primary particles are formed in the eutectic bed. Morphologies of the brazed layer could be controlled by changing the composition of the amorphous filler metal. $Zr_{0.7}Be_{0.3}$ amorphous alloy is the most probable filler metal for the joining of Zr alloys in the viewpoint of corrosion resistance.

References

[1] R.D. Page, AECL-5609, Canadian Power Reactor Fuel, 1976.
[2] G. Mcgregor, Process for brazing zirconium alloy elements, Canadian Patent No. 883578, 1971.
[3] P.J. Apencer, O.V. Goldbeck, Beryllium Physicochemical Properties of its Compounds and Alloys, Atomic Energy Review, 1978.
[4] J. Amato, F. Baudrocco, M. Ravizza, Welding J. 51 (7) (1972) 341.
[5] N. Bredz, H. Sdhwartzwart, Welding J. 37 (8) (1959) 305.
[6] K.T. Bates, AECL-2813, Brazing of Zircaloy in nuclear fuel, 1966.
[7] L.E. Tanner, R. Ray, Acta Metall. 27 (1979) 1727.
[8] G.F. Syrykh, A.P. Zhernov, M.N. Kholopkin, A.V. Suetin, J. Non-Cryst. Solids 181 (1995) 244.
[9] A.M. Bratkovsky, S.L. Isakov, S.N. Ishmaev, I.P. Sadikov,

A.V. Smirnov, F.G. Syrykh, M.N. Hlopkin, N.A. Chernoplekov, J. Non-Cryst. Solids 156–158 (1993) 72.
[10] R. Hasegawa, L.E. Tanner, Phys. Rev. B 16 (9) (1977) 3925.
[11] N.J. De Cristofaro et al., Welding J. 57 (7) (1978) 33.
[12] D. Bose, A. Datta, Welding J. 60 (10) (1981) 29.
[13] N.J. De Cristofaro, A. Datta, Rapidly Quenched Metals (1985) 1715.
[14] P. Duwez, Trans. Am. Soc. Metals 60 (1967) 607.
[15] R.W. Cahn, P. Hassen (Eds.), Physical Metallurgy, Elservier Science, Amsterdam, 1983.
[16] Powder diffraction files, JCPDS, International Center of Diffraction Data, 1994.
[17] H.E. Kissinger, Anal. Chem. 29 (1957) 1702.
[18] T.B. Massalski (Ed.), Binary Alloy Phase Diagrams, 2nd ed.
[19] E.A. Brandes, G.E. Brook (Eds.), Smithells Metals Reference Book, 7th ed.
[20] D.G. Hardy, N.A. Graham, The performance, strength and corrosion resistance of brazed joints on CANDU fuel bundles, Trans. ANS 19 (1974).